International Journal of Mechanical Sciences 182 (2020) 105745

Contents lists available at ScienceDirect

International Journal of Mechanical Sciences

journal homepage: www.elsevier.com/locate/ijmecsci

Size dependent electro-elastic enhancement in geometrically anisotropic lead-free piezocomposites

Jagdish A. Krishnaswamy [a,*], Luis Rodriguez-Tembleque [b], Roderick Melnik [a,b], Federico C. Buroni [c], Andres Saez [b]

[a] MS2Discovery Interdisciplinary Research Institute, Wilfrid Laurier University, 75 University Ave W, Waterloo, Ontario N2L 3C5, Canada
[b] Department of Continuum Mechanics and Structural Analysis, Universidad de Sevilla, Camino de los Descubrimientos s/n, Seville E-41092, Spain
[c] Department of Mechanical Engineering and Manufacturing, Universidad de Sevilla, Camino de los Descubrimientos s/n, Seville E-41092, Spain

ARTICLE INFO

Keywords:
Flexoelectricity
Size-dependent piezoelectricity
Coupled models
Finite element analysis
Lead-free piezocomposites
Electrostriction

ABSTRACT

Improving the performance of lead-free piezocomposites to the levels of state-of-the-art lead-based composites has been an important challenge in composite research. Consequently, an important agenda of piezocomposite research has been to identify new coupled mechanisms that can enhance the piezoelectric response. One such method is to tap into the size-dependent flexoelectric phenomenon in geometrically anisotropic structures. Numerical models which can account for flexoelectricity and nonlinear effects such as electrostriction are not well-developed for piezocomposite design, and current designs are based on linear piezoelectric models. Here, we develop an advanced model with flexoelectric and electrostrictive contributions in geometrically tailored piezocomposites to obtain insights on aspects of enhanced response due to small-size effects. Here, based on design considerations, we numerically demonstrate that in epoxy-matrix-based piezocomposites which are structured as truncated pyramids, flexoelectricity can lead to significant enhancements in both the electric field and the electric flux generation at small length scales. Particularly, we show that at dilute inclusion concentrations, dramatic improvements nearing 150% in the piezoelectric response are possible. Further, the flexoelectric enhancement is sensitive to the packing of the inclusions within the composite structure with the best enhancements occurring when the inclusions are closer to the inclined edges of the pyramids. We also show that in composite structures with CNT-modified matrices, flexoelectricity produces similar enhancements as in the case of unmodified matrices, demonstrating that the effect operates almost independent of nanoscale elastic and dielectric modifications by the nanotubes. Finally, we also establish that for a large range of applied stresses, the nonlinear deviations in the response due to electrostriction are negligible and flexoelectricity is the predominant size-dependent enhancement mechanism in structured lead-free piezocomposites.

1. Introduction

Although lead-free piezocomposites represent an important green alternative to current lead-based composites, the performance of these composites still lags the state-of-the-art materials [1,2]. This gap in the performance can be bridged by a number of well-understood design strategies. These approaches include nanomodification to harden the matrix and to improve its permittivity [3] and tuning the polycrystallinity of the piezoelectric inclusions [4]. While these approaches are effective, they still require the addition of a new material to the composite. There is another path to improve the piezoelectric response, which is by exploiting various electro-elastic coupled processes, in addition to conventional linear piezoelectric coupling. This path can lead to pronounced enhancements with no requirement of adding new materials into the composite and the resulting design being amenable to scalable manufacturing by emerging processes such as 3D printing. Among such coupled processes, an important role is played by flexoelectricity, which couples the components of the gradients of strain and the electric field [5,6]. The importance of this mechanism stems from the fact that flexoelectricity, unlike linear piezoelectricity, occurs even in centrosymmetric materials [5,6] and therefore represents a mode of electricity generation purely from strain gradients in a larger class of materials. Experiments have demonstrated that paraelectric crystals can exhibit significant flexoelectric coefficients [6]. Particularly, lead free materials such as $BaTiO_3$ (Barium titanate) and BST (Barium strontium titanate) exhibit relatively large flexoelectricity compared to lead-based perovskite crystals [7–9].

One of the straightforward and well-understood ways to harness electricity through flexoelectricity was to build anisotropic geometries,

* Corresponding author.
E-mail address: ajagdish@wlu.ca (J.A. Krishnaswamy).

https://doi.org/10.1016/j.ijmecsci.2020.105745
Received 19 January 2020; Received in revised form 5 April 2020; Accepted 1 May 2020
Available online 22 May 2020

such as truncated pyramids (or truncated triangles in two dimensions) which, on account of the directionally oriented structure subject to a stress, can introduce large strain gradients and excite flexoelectric processes [10–12]. Experiments on the paraelectric phase of many crystals such as barium-strontium titanate [13–15] have reported significant flexoelectric generation through geometrical tuning of the sample. This is also a theoretically well-understood problem with both analytical and computational efforts clearly showing that flexoelectric processes in such anisotropic structures can exhibit size-dependence, with smaller length scales having more pronounced flexoelectric generation due to amplified strain gradients [10,11,16]. These effects have also been explored in the context of defective nanostructured materials which possess anisotropy and consequent flexoelectric behavior [17,18]. Also, based on recent efforts, size-dependent effects are of particular interest in composite materials [19–21]. However, most of these studies are conducted on a single material having a paraelectric phase. The implications of such geometric tuning in the context of the structure of piezoelectric composites with ferroelectric inclusions, where linear piezoelectricity and flexoelectricity can coexist and interact, is not a well-addressed problem. Although there are a few reports that look into the flexoelectric processes in composites with matrices and inclusions [22], these are preliminary in nature, with little focus on the optimization of composite performance based on size-dependent behaviors. The other composite architectures investigated for their flexoelectric behavior, including recent efforts, consist of geometries comprised of a one dimensional stacking of materials [23,24]. While these current studies are focused on simple architectures and material configurations, flexoelectricity in a higher dimensional composite architecture is still scarcely explored. Also, most of the computational results obtained in this area considers the piezoelectric and the flexoelectric models separately. However, it is known that it is possible for the flexoelectric and piezoelectric effects to counteract with each other through destructive interplays and it is important to understand the conditions under which both effects operate synergistically [25]. It is therefore the central agenda of this paper to investigate size dependent flexoelectric enhancements in piezoelectric composites within the context of a unified mathematical model which considers both the piezoelectric and flexoelectric effects together. Further, it is also known that higher order nonlinear effects such as electrostriction can show significant strain-dependent deviations from the predictions of linear electro-elastic models [26]. Electrostriction is a phenomenon that couples two components of the electric field with a component of strain [26–28], which can lead to nonlinear deviations in the effective material coefficients with respect to the predictions of the linear models. Therefore, the coupled electro-elastic model developed here simultaneously takes into account both the essential phenomena – flexoelectricity and electrostriction – in addition to linear piezoelectricity, to investigate the size-dependent enhancements occurring in the response of geometrically anisotropic lead-free piezocomposites.

In the following sections, we first provide the details of the composite architecture, the electro-elastic coupled model and the boundary conditions, and the material properties. This is followed by the discussion and summary of the results.

2. Electro-elastic model and material properties

In this section, we will provide the details of the electro-elastic model describing composite behavior, followed by a discussion of the material properties.

2.1. Electro-elastic model

In this section, we will develop the constitutive relations and governing laws of electro-elastic coupling including the effects of linear piezoelectricity, flexoelectricity, and electrostriction. The Gibbs free energy density in terms of the electric fields E_i strains ε_{ij}, and strain gradients $\varepsilon_{ij,k}$ is given by [22,23,27,28]:

$$G = \frac{1}{2}c_{ijkl}\varepsilon_{ij}\varepsilon_{kl} - \frac{1}{2}\varepsilon_{ij}E_iE_j - e_{kij}E_k\varepsilon_{ij} - \frac{1}{2}B_{klij}E_kE_l\varepsilon_{ij} - \mu_{ijkl}E_i\varepsilon_{jk,l}, \tag{1}$$

where c_{ijkl}, ε_{ij}, e_{ijk}, B_{ijkl}, and μ_{ijkl} are the elastic, permittivity, piezoelectric, electrostrictive, and flexoelectric coefficients, respectively. From Eq. (1) we obtain the phenomenological relationships describing for the stress σ_{ij}, higher order stresses $\hat{\sigma}_{ijk}$, and the electric flux density D_i, as follows:

$$\sigma_{ij} = \frac{\partial G}{\partial \varepsilon_{ij}} = c_{ijkl}\varepsilon_{kl} - e_{kij}E_k - \frac{1}{2}B_{klij}E_kE_l, \tag{2a}$$

$$\hat{\sigma}_{ijk} = \frac{\partial G}{\partial \varepsilon_{ij,k}} = \mu_{lijk}E_l, \tag{2b}$$

$$D_i = -\frac{\partial G}{\partial E_i} = \varepsilon_{ij}E_j + e_{ijk}\varepsilon_{jk} + B_{ijkl}E_j\varepsilon_{kl} + \mu_{ijkl}\varepsilon_{jk,l}. \tag{2c}$$

Further, the balance laws which govern the composite behavior are given by [23]:

$$\left(\sigma_{ij} - \hat{\sigma}_{ijk,k}\right)_{,j} + F_i = 0, \tag{3a}$$

$$D_{i,i} = 0, \tag{3b}$$

where F_i represent the components of body force which are assumed to vanish. In the absence of higher order stress components $\hat{\sigma}_{ijk}$, Eq. (3a) would reduce to the balance of linear momentum in the classical elastic formalism [23]. As pointed out in [23], the higher order stresses can be interpreted as moment stress and the balance equation could be thought of as including the balance for linear and angular momenta.

The composite geometry and the boundary conditions adopted for the analysis are explained in detail in Section 3. (For a quick reference, please see Fig. 1(a) and (b) for the geometrical details of the composite and the boundary conditions applied for the analysis. More detailed explanation is provided in Section 3). The electro-elastic model discussed here, in conjunction with the boundary conditions applied on the geometrically tailored composite architecture, are analyzed using the finite element analysis using COMSOL Multiphysics software. Details of the finite element mesh are provided in the appendix A1.

2.2. Material properties

We consider epoxy/$BaTiO_3$ lead free piezoelectric composites. Epoxies, widely used as matrices for piezoelectric fillers, could serve as a standard representative example of matrix materials [29,30]. The inclusions, which are randomly shaped and positioned, are assumed to be composed of single-crystal $BaTiO_3$ poled along the x_3 direction. The elastic, dielectric, piezoelectric, flexoelectric, and electrostrictive properties of these materials are summarized in Table 1. Voigt notation has been used for indexing the coefficients. The electrostrictive coefficients are typically described in two forms – in terms of strain-polarization coupling and strain-electric field coupling. This gives rise to two forms of electrostrictive coefficients - Q_{ijkl}(m^4C^{-2}) and M_{ijkl} (m^2V^{-2}). Material data which is available in one of these two forms is interconvertible using the relation $M_{ijkl} = Q_{opkl}\eta_{oi}\eta_{pj}$, where η_{ij} refer to the components of the electrical susceptibility tensor. Following this, the M_{ijkl} coefficients are converted into a form required by Equation (2) using $B_{ijkl} = c_{ijpq}M_{pqkl}$. Further, the flexoelectric tensor is assumed to have three components: a longitudinal ($\mu_{11} = \mu_{33}$), a transverse (μ_{13}), and shear (μ_{44}) components. Since the shear components are not well-characterized [11], we assume $\mu_{44} = 0$. The electric flux density generated by the longitudinal and transverse flexoelectric effects are related to the strain components as given by $D_{1,flexo} = \mu_{11}\varepsilon_{11,1} + \mu_{13}\varepsilon_{33,1}$ and $D_{3,flexo} = \mu_{13}\varepsilon_{11,3} + \mu_{11}\varepsilon_{33,3}$ [31].

The parameters λ_m and μ_m are the Lame's parameters for the elastically isotropic matrix, given by $\lambda_m = \frac{E_m\nu_m}{(1+\nu_m)(1-2\nu_m)}$ and $\mu_m = \frac{E_m}{2(1+\nu_m)}$.

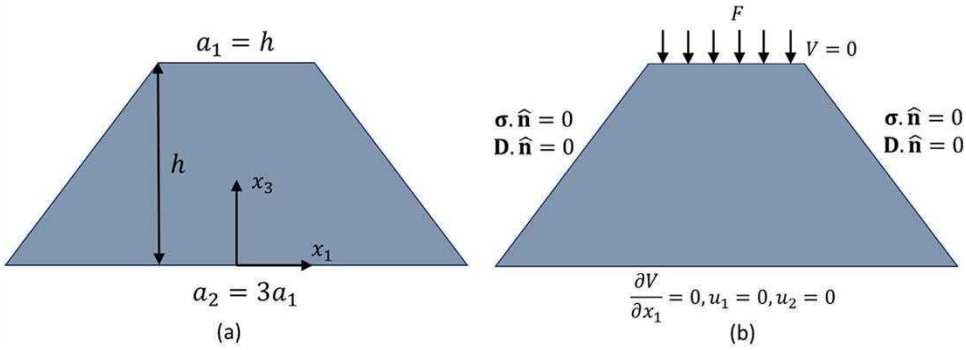

Fig. 1. (a) The truncated pyramid piezocomposite in two dimensions with its important geometric parameters and the coordinate system, (b) the boundary conditions applied to determine the electro-elastic behavior of the composite structure.

Table 1
Electro-elastic material coefficients adopted in this study.

Material property Elastic coefficients (Moduli in Pa)	Values for $BaTiO_3$	Values for epoxy matrix
c_{11}	275.1×10^9 [32]	$\lambda_m + 2\mu_m$
c_{13}	151.55×10^9	λ_m
c_{33}	164.8×10^9	$\lambda_m + 2\mu_m$
c_{44}	54.3×10^9	μ_m
Young's modulus, E_m	N.A.	1×10^9 [33] (typical value)
Poisson's ratio, ν_m	N.A.	0.35
Relative permittivity		
ϵ_{11}/ϵ_0	1970 [32]	3.5 [33]
ϵ_{33}/ϵ_0	109	3.5
Piezoelectric coefficients (Cm^{-2})		
e_{15}	21.3 [32]	Matrix is
e_{31}	− 2.69	non-piezoelectric
e_{33}	3.65	
Flexoelectric coefficients (Cm^{-1})		
Longitudinal, μ_{11}	1×10^{-6} [8,11,22]	1×10^{-9} [34]
Transverse, μ_{12}	1×10^{-6} [9,11,22]	1×10^{-9}
Shear, μ_{44}	0	0
Electrostrictive coefficients, $\mathbf{Q_{ijkl}}$ ($\mathbf{m^4C^{-2}}$) or $\boldsymbol{M_{ijkl}}$($\mathbf{V^{-2}m^2}$)		
Longitudinal	0.1 m^4C^{-2} [35]	1×10^{-17} $V^{-2}m^2$ [36]
Transverse	− 0.034 m^4C^{-2}	0
Shear	$0.29m^4C^{-2}$	0

Further, we also consider the case where the matrix is modified by the addition of (15,15) multiwalled carbon nanotubes (MWCNTs). The nanoaddition brings about hardening in the matrix and also increases its permittivity, both of which improve the piezoelectric response through better mechanical coupling and electric flux transport [3]. The objective of this part of the investigation is to study the effects of flexoelectricity in piezocomposites with nanomodified matrices, which represent a well-studied family of high-performance piezocomposites. The effective elastic properties of the modified matrices are provided in the appendix A2. These effective properties are derived by micromechanics methods described in [37]. For small CNT additions, the elastic coefficients c_{ijkl} increase linearly with the CNT concentration f_{CNT}. Further, the effective permittivity of the matrix also increases with a percolative dependence on the CNT concentration, given by $\epsilon_M^{eff} = \epsilon_M (\frac{f_p}{f_p - f_{CNT}})^p$ [38,39], which means that the effective permittivity of the matrix escalates to very large values as $f_{CNT} \to f_p$. In this relation, ϵ_M is the relative permittivity of the pristine matrix, f_p is the percolation threshold for the nanotubes within the matrix, and p is the critical exponent characterizing the percolation behavior. Typical values for carbon nanotubes with an aspect ratio (= $l/2r$) of 100, assuming no agglomerations, are around $f_p = 0.7\%$ [40] and $p = 1.0$ [41]. We use these values in our analysis.

Table 2
Material properties for $BaTiO_3$ for validating the model, chosen in accordance with [11].

Property	Value
Young's modulus, E_{BTO}	100 Gpa
Poisson's ratio, ν	0.37
Flexoelectric coefficient, $\mu_{13} = \mu_{11}$	1 μC/m
Permittivity	11.0 nC/Vm
ϵ_{33}	12.48 nC/Vm

3. Results and discussions

We will proceed by first verifying our model (Section 3.1) and sequentially look at size scale effects in particular piezoelectric composites (Section 3.2), the relation between inclusion concentration and flexoelectric enhancement (Section 3.3), and the role of the inclusion packing and localization within the pyramid in determining the total piezoelectric and flexoelectric response.

3.1. Model validation

We will first verify the model developed here by comparing its results with standard literature data. The flexoelectric effect has been studied earlier in the context of a truncated pyramid geometry [11]. In this case, the material is assumed to be paraelectric $BaTiO_3$. It has a cubic unit cell and hence no ferroelectric behavior. Electric flux generation, therefore, can occur only due to strain gradients, the effects of which are amplified when the material geometry itself possesses a spatial gradient. The geometry of the pyramid is shown in Fig. 1(a), with the geometrical parameters $a_1 = \frac{a_2}{3} = h$. We choose $h = 75$ μm. The geometry is further scaled using a scaling parameter N, and the parameters of the scaled geometry are Na_1, Na_2, and Nh. Fig. 1(b) further shows the boundary conditions used in the investigation. By this definition, N is the normalized thickness of the truncated geometry considered here. The broader side of the pyramid is held rigid and further acts as an electrode ($\frac{\partial V}{\partial x_1} = 0$). The narrower side of the pyramid is electrostatically grounded ($V = 0$) and is subject to a force F. The inclined boundaries on the side of the pyramid are free (no tractions and no electric flux normal to the boundary). These boundary conditions are used throughout this analysis.

Table 2 shows the electro-elastic properties of paraelectric $BaTiO_3$ which are used for these simulations. The material is elastically isotropic and is characterized by its Young's modulus and Poisson's ratio. Further, we assume that the force is given as $F = 4.5$KN. Fig. 2(a) and (b) show the spatial distribution of the strain component ϵ_{33} and the electric potential V for $N = 1$, i.e. $h = a_1 = \frac{a_2}{3} = 75$ μm. These predictions are in good agreement with the results reported in literature [11]. Further, the scaling parameter is varied to evaluate the size-effect of the flexoelectric response, which is known to escalate at small size scales. The response is quantified in the form of an effective piezoelectric coefficient given

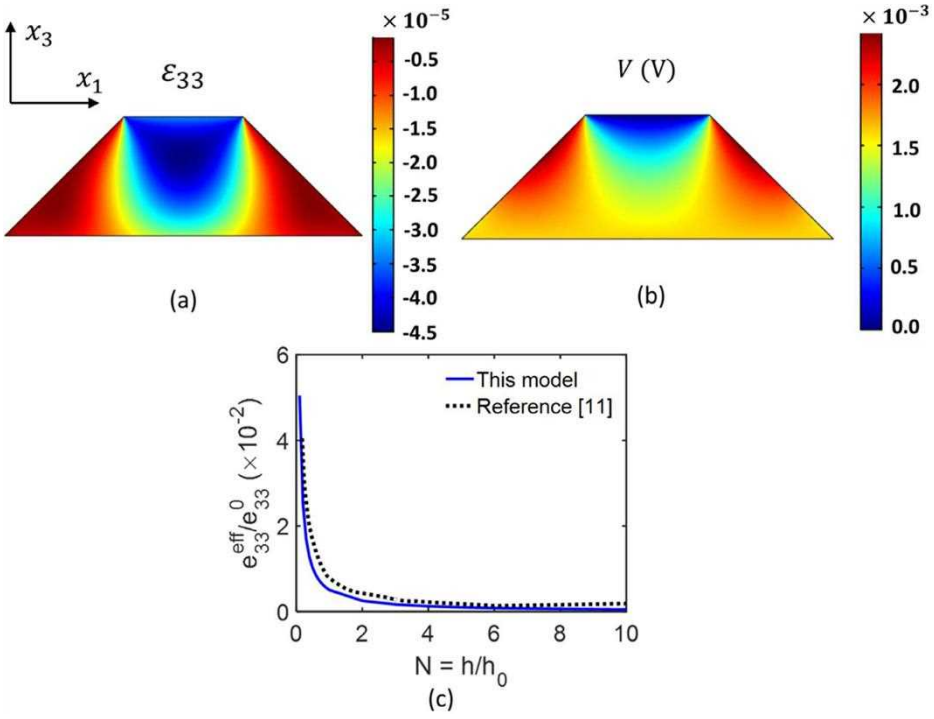

Fig. 2. Verification of standard flexoelectric numerical predictions assuming the truncated structure to be composed of paraelectric $BaTiO_3$. (a) and (b) show the distribution of the strain component ε_{33} and the electric potential V, and (c) shows the predicted size-dependent enhancement in the effective piezoelectric coefficient of the structure, as a function of the scaling parameter N. These results show close agreement with the predictions made in literature [11].

by [11]

$$e_{33}^{eff} = \frac{\varepsilon_{33} V a_2 c_{11}}{hF} \tag{4}$$

This is further normalized with the normalization parameter $e_0 = 4.4\ \mathrm{Cm}^{-2}$ and the results are plotted in Fig. 2(c). It is clear that the model developed here predicts the known size scale effect of the flexoelectric effect and the predictions show good agreement with the data in the literature [11].

3.2. Size-dependent flexoelectric enhancement in lead-free particulate piezocomposites

We have validated the flexoelectric model in the previous section. Here we will proceed by studying the coupled effects of linear piezoelectricity and flexoelectricity when the pyramid is made of a lead-free piezocomposite material. The $BaTiO_3$ inclusions are now anisotropic, unlike in Section 3.1, and have ferroelectric (and linear piezoelectric) behavior in addition to flexoelectricity. We consider 8 composite structures with an inclusion concentration $V_{BTO} = 17\%$ ($\pm$ 6.4% relative error). The geometrical parameters and the scaling procedure of the truncated pyramid is similar to that described in Section 3.1 and Fig. 1. The inclusions are randomly shaped and are confined within two concentric circles of radii $R_1 = h/5$ and $R_2 = 0.75R_1$, which obey the same scaling rules. To compare the size dependence in the case of this anisotropic composite architecture, we consider the following quantities:

$$g_{33}^{eff} = \left| \frac{V_{bottom} - V_{top}}{\sigma_{33} h} \right| \tag{5}$$

$$d_{33}^{eff} = \frac{e_{31}\varepsilon_{11} + e_{33}\varepsilon_{33} + \mu_{3113}\varepsilon_{11,3} + \mu_{3333}\varepsilon_{33,3}}{A\sigma_{33}} \tag{6}$$

These are the effective electric field coefficient and the effective piezoelectric coefficient, respectively, of the composite structure, calculated by assuming it to be a rectangular block of width a_2 and height h. These calculations are done in accordance with the procedures reported in [11]. These quantities can be thought of as effective performance parameters if the pyramid is replaced with homogenous material of having a rectangular shape. Accordingly, $\sigma_{33} = F/a_2$. Both of these quantities need to be maximized in order to maximize the energy density in the composite [2]. In evaluating the flexoelectric enhancement, the coefficients g_{33}^{eff} and d_{33}^{eff} will be normalized by the values of the coefficients evaluated without flexoelectric contribution for $N = 1$. These reference values are denoted g_{33}^{0} and d_{33}^{0} and they serve as normalization parameters.

To verify the size-dependent behavior, we plot the effective electric field coefficient g_{33}^{eff} as a function of the scaling parameter N, averaged over the 8 composite structures illustrated in Fig. 3(a). We notice that while the linear piezoelectric model predicts no size-dependence (Fig. 3(b)), the flexoelectric model for the composite predicts that there is indeed flexoelectric enhancement in the electric field coefficient (Fig. 3(c)). Further, the enhancement in g_{33}^{eff} can exceed 20% (Fig. 3(d)) at small size scales ($N \sim 10^{-2}$). The enhancement in the effective flux generation, characterized by the effective piezoelectric constant d_{33}^{eff}, also exceeds 10%, for this inclusion volume fraction (Fig. 3(e)). This proves that in piezoelectric composite materials with geometric anisotropy, flexoelectric enhancement can be a mode of improving the performance. Further, as pointed out in earlier studies [10], further improvements in the flexoelectric coupling are possible by tweaking the area ratio $R = (a_2/a_1)^2$ of the pyramid.

3.3. Flexoelectric enhancement in piezocomposites with CNT-modified matrices

Adding nanomaterials such as carbon nanotubes is a well-understood method of enhancing the performance of a piezocomposite through hardening of the matrix and improvement in its permittivity [3]. It is, therefore, also important to understand the role of flexoelectric enhance-

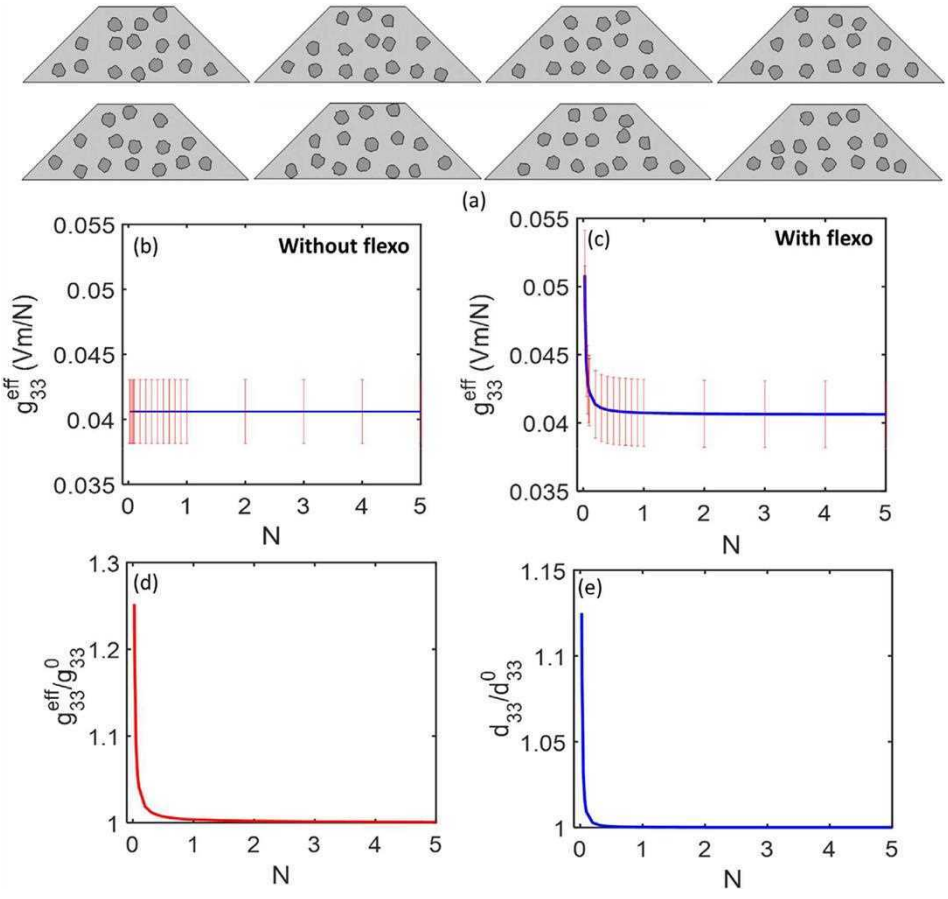

Fig. 3. (a) 8 piezocomposite architectures with similar inclusion concentrations ($V_{BTO} \approx 17\%$) used for statistically evaluating the size dependent piezoelectric effect, (b) and (c) show the effective electric field coefficient g_{33}^{eff}, averaged over the 8 structures, with and without flexoelectric contributions, respectively. (d) and (e) show the averaged size-dependent enhancements in the effective coefficients g_{33}^{eff} and d_{33}^{eff}, respectively, as a function of the scaling parameter N.

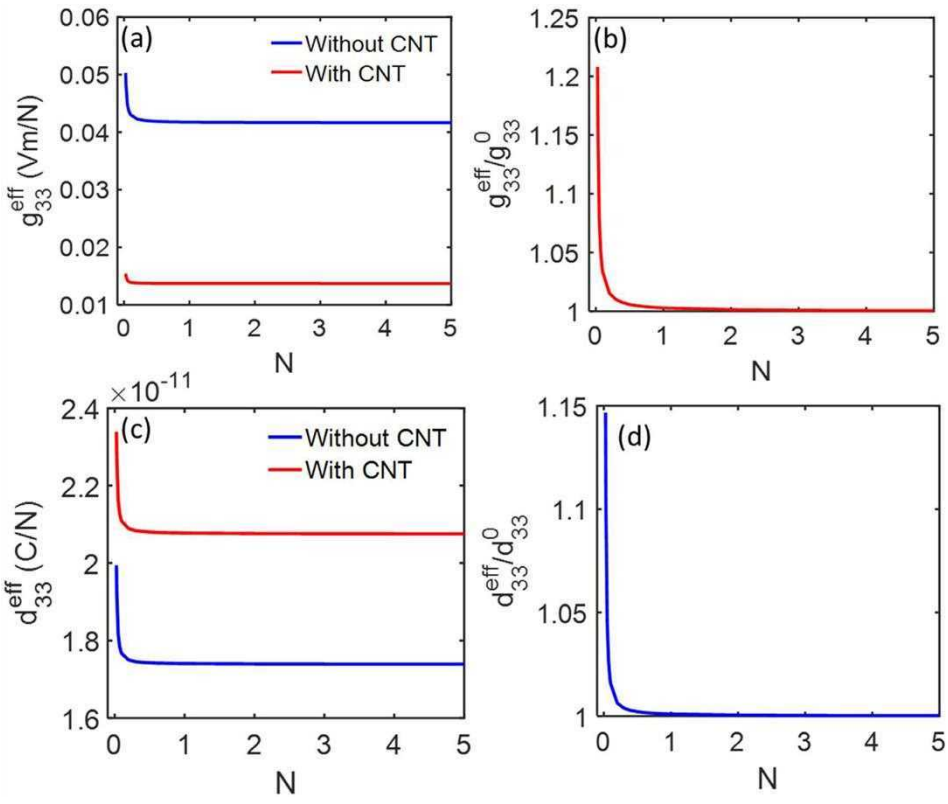

Fig. 4. Size dependent effects with CNT-modified matrices as a function of the scaling parameter N. (a) the effective electric field coefficient with and without nanomodification in the matrix, (b) the size-dependent enhancement in g_{33}^{eff} with a nanomodified matrix, (c) the effective piezoelectric coefficient with and without nanomodification in the matrix, (d) the size-dependent enhancement in d_{33}^{eff} with nanomodified matrix.

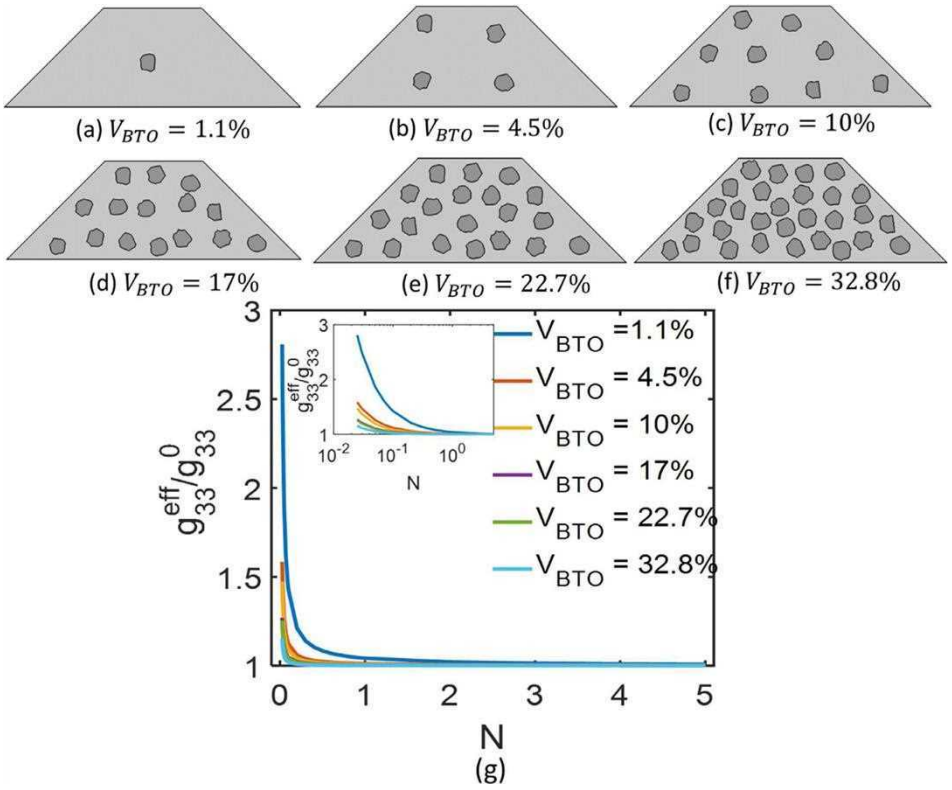

Fig. 5. The effect of inclusion concentration on the size-dependent flexoelectric enhancement. (a)-(f) show composite structures with progressively increasing inclusion concentration V_{BTO}, (g) shows the flexoelectric size-dependent enhancement in the effective electric field coefficient g_{33}^{eff} as a function of the scaling parameter N.

ment in such nanomodified composites, to identify possible routes of enhanced performance.

Particularly, we are interested in identifying coupled effects between the size-dependent flexoelectricity and the nanoscale modification of the matrix hardness and permittivity. Although carbon nanostructures have been shown to exhibit flexoelectric behavior, considering the geometry of CNTs, theoretical studies have shown the absence of flexoelectric behavior [42]. Secondly, the microstructure of the matrix we consider does not have any geometrical anisotropy (for example, aligned nanotubes). Hence, we expect that although there could be some flexoelectricity due to individual nanotubes, the random orientation of the nanotubes results in no net flexoelectricity. The requirement of having geometric anisotropy for a material to exhibit flexoelectricity is emphasized in [23]. Therefore, we assume the flexoelectric coefficients of the modified matrix to be the same as the pristine matrix, to a first approximation (i.e. $\mu_{11} = \mu_{13} = 1 \times 10^{-9}$ Cm^{-1}). Further, the addition of CNTs hardens the matrix and also increases the permittivity. For this case, we consider the matrix material to be the epoxy, araldite LY5052, the elastic properties of which are $E_m = 3.5$ GPa and $\nu_m = 0.35$. As mentioned in Section 2.2, further details on the effective elastic and dielectric properties of the nanomodified matrix are provided in the appendix. We first compare the performance of the composite structures with the pristine and the nanomodified matrices. We see that the effective piezoelectric coefficient, d_{33}^{eff}, of the nanomodified composite is notably higher than the reference architecture without CNTs (Fig. 4(a)). However, the electric field coefficient, g_{33}^{eff}, is lesser in the nanomodified composite (Fig. 4(c)). This is because while nanomodification allows higher flux generation, it comes at the cost of an increased permittivity, which reduces the electric fields built up within the material. However, we note that both the coefficients have flexoelectric enhancements at lower size scales. Particularly, the size-dependent enhancements in d_{33}^{eff} and g_{33}^{eff} (Fig. 4(b) and (d), respectively) are similar to the improvements seen in the piezocomposites with pristine matrices. This observation suggests that the coupling between flexoelectricity and nanoscale electro-elastic changes occurring due to addition of nanomaterials might not be very significant and that the flexoelectric effect could be an independent size-dependent enhancement mechanism in composites of the type considered here.

3.4. Effect of inclusion concentration and spatial packing

We will next look at the effect of the inclusion concentration V_{BTO} on the flexoelectric enhancement. We consider six different composite geometries with increasing inclusion concentrations as illustrated in Fig. 5(a)–(f). The normalized effective electric field coefficient of these composite geometries is plotted in Fig. 5(g). We see that the composite with the least inclusion concentration has maximum flexoelectric enhancement at smaller size scales, with the enhancement exceeding 150% in the electric field coefficient. The flexoelectric enhancement decreases as the inclusion concentration increase. From the perspective of the designing devices for specific applications, this is an interesting observation that offers a route to drastically enhance the performance of a piezocomposite with dilute inclusion concentrations. Such composites are relatively softer and are suited for flexible electronic and wearable applications [43,44].

We look at another important aspect of design – the one which arises due to the way in which the inclusions are spatially distributed within the truncated pyramid. Given the anisotropy of the shape, the positioning of inclusions might be an important parameter to consider while designing the material and optimizing the manufacturing process. We consider a composite architecture with 15 inclusions in three configurations as shown in Fig. 6(a)–(c). In the first case, we assume that the inclusions are uniformly distributed within the matrix (Fig. 6(a) - uniform). In the second, case, we assume the inclusions are packed together

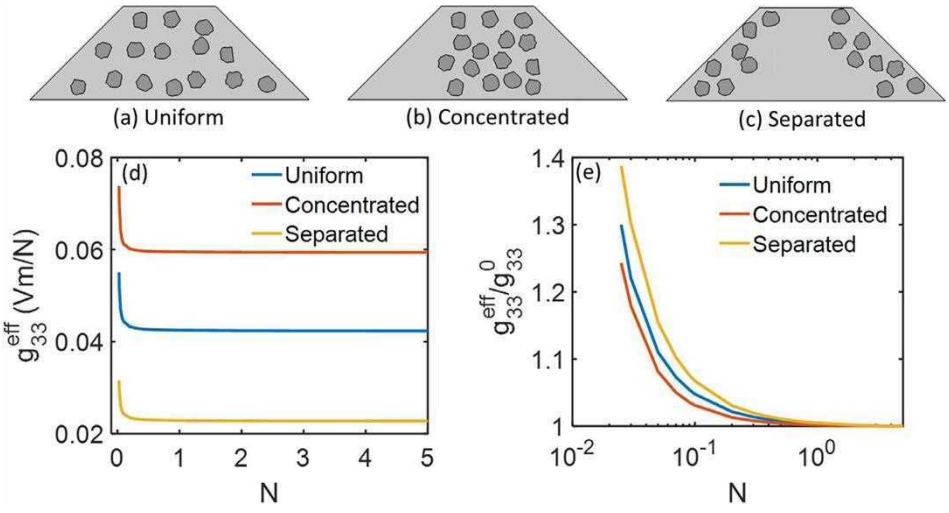

Fig. 6. The effect of inclusion packing and positioning within the composite structure on flexoelectric behavior. (a)–(c) Show three composite structures with inclusion volume fractions ($V_{BTO} \approx 17\%$), but different packing configurations, (d) shows the effective electric field coefficient of the three structures as a function of N, and (e) shows the size-dependent enhancement in g_{33}^{eff} for the three structures.

in the central region of the truncated pyramid (Fig. 6(b) - concentrated), and in the third case, we assume that the inclusions are separated out and are found near the edges of the truncated pyramid (Fig. 6(c) - separated).

From the values of the computed g_{33}^{eff} plotted in Fig. 6(d), we observe that the best response is obtained from the configuration in which the inclusions are concentrated in the central portion of the truncated pyramid and the least response occurs in the separated configuration. This is mainly because the applied stress is mostly concentrated below the top face of the pyramid and therefore most of the linear-piezoelectric generation due to homogeneous strain occurs in this region. Therefore, this configuration is optimal for the best linear piezoelectric response, as seen from Fig. 6(d), even for large N. The flexoelectric enhancement at small sizes is seen in all three configurations. However, the flexoelectric enhancement tends to slightly increase as the inclusions are moved away from the center of the truncated pyramid (Fig. 6(e)). This suggests that the flexoelectric activity is relatively larger towards the inclined edges of the pyramid. This is because the geometric anisotropic of the composite structure spatially localizes large strain gradients towards the edges of the tapered structure, therefore making it a region of relatively larger flexoelectric generation compared to the central regions. This study shows that it is possible to tune both the piezoelectric and the flexoelectric characteristics of a composite by tweaking the spatial distribution of the inclusions within the pyramid. For example, an efficient material design could involve development of optimal spatial distributions of inclusions to maximize the flexoelectric enhancement while also retaining high piezoelectric response. This could be important in designing arrays of such pyramids with gradient electro-elastic characteristics that could allow significant anisotropy and hence be useful in the areas such as, for example, directional strain sensing.

3.5. Nonlinear contributions to electro-elastic response

We further consider an important aspect of electro-elastic behavior – that of nonlinear electro-elastic coupling. Particularly, we look at electrostriction where the two components of strain are coupled to a component of the electric field. It is possible that electrostriction can lead to non-linear deviations from the linear behavior, with the deviations becoming more significant with larger applied stimuli. The electrostrictive coefficients of the materials are summarized in Table 1. Conversion of these parameters into a form compatible with the constitutive relations Eq. 2(a)-(c) is done as outlined in [27], and explained in Section 2.2. Specifically, we have $M_{ijkl} = Q_{opkl}\eta_{oi}\eta_{pj}$, where η_{ij} refer to the components of the electrical susceptibility tensor. Following this, we convert these coefficients to the form required by Equation (2) using $B_{ijkl} = c_{ijpq}M_{pqkl}$. We consider a scaled geometry with $N = 0.03$, where flexoelectric contributions are significant and we assume an inclusion concentration of $V_{BTO} = 17\%$, as illustrated in Fig. 7(a). For various applied stresses ($\sigma = F/a_1$), we calculate g_{33}^{eff} and d_{33}^{eff} of the composite. In the absence of nonlinear behavior, these materials are expected to be invariant with respect to the applied stimulus, as verified by the results in Fig. 7(b) and (c). However, in the presence of electrostrictive nonlinearities, these properties are stimulus-dependent. Specifically, g_{33}^{eff} and d_{33}^{eff} show weak reduction and enhancement, respectively, as the applied stress increases. Given the weak dependence of these parameters on the applied stimulus, the electrostriction-induced nonlinear deviations can be neglected, to a first approximation, from the material design considerations. It is therefore anticipated that in piezocomposites structured as truncated pyramids, the major source of performance enhancement is the nonlocal contribution due to flexoelectricity and not due to nonlinear contributions.

4. Summary

We have demonstrated that, in lead-free particulate piezoelectric composites, flexoelectricity could play a significant role in electromechanical conversion, when the composite material possesses geometric anisotropy. An illustrative demonstration of this was provided by structuring the composite material as a truncated pyramid. We have shown that flexoelectric enhancements, at small size scales, are significant for both the electric fields and the electric polarization due to applied stresses. Further, this enhancement more significant for smaller inclusion concentrations, whereby notable enhancements exceeding 150% were demonstrated, in the effective electric field. Moreover, the flexoelectric enhancement and overall performance of the composite structure is shown to be sensitive to the packing and positioning of the inclusions within the truncated pyramid. We also analyzed the flexoelectric enhancement in such composite structures with a CNT-modified matrix. The nanomodified designs showed similar flexoelectric enhancements in the electric flux generation as the reference designs. However, the flexoelectric enhancements in the electric field generation were slightly lesser in the nanomodified designs. Finally, we have also evaluated the contribution of nonlinear effects, particularly that of electrostriction. We see that the nonlinear stress-dependent deviations of the material behavior are negligible and the major source of enhancement at small

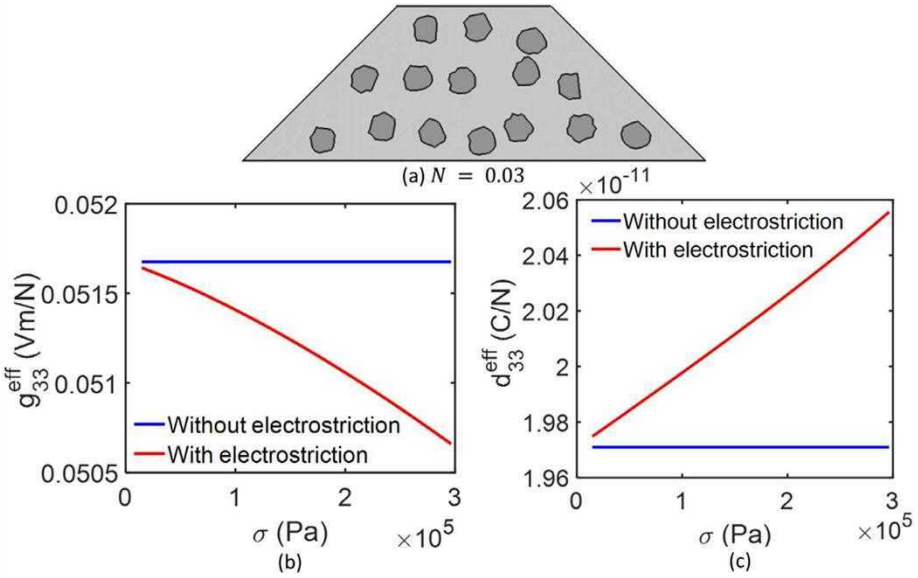

Fig. 7. (a) the composite architecture with $N = 0.03$ and $V_{BTO} = 17\%$ chosen for analyzing the contribution of electrostriction at small length scales, (b) the effective electric field coefficient and (c) the effective piezoelectric coefficient, with and without electrostriction, as a function of applied stress (following boundary conditions in Fig. 1(b).

size scales is that due to flexoelectricity only. Overall, the advanced modelling paradigm developed here, to consider the various important modes of electro-mechanical coupling including linear piezoelectricity, flexoelectricity, and electrostriction, clearly allows the prediction of size dependent piezoelectric enhancements and the design of geometrically tailored composites with superior performance.

Authors statement

JAK did the finite element calculations and prepared the initial draft of the manuscript. LRT did the calculations of effective elastic properties, based on the two-parametric model for the CNT-modified matrix materials. AS and RM designed research and contributed to all its aspects. All authors reviewed the manuscript and gave approval to its final version.

Declaration of Competing Interest

The authors declare that they have no known competing financial interests or personal relationships that could have appeared to influence the work reported in this paper.

Acknowledgements

This work was supported by the Ministerio de Economía y Competitividad of Spain and the European Regional Development Fund under projects RTI2018-094945-B-C21 and DPI2017-89162-R. The financial support is gratefully acknowledged. RM and AKJ are also grateful to the NSERC and CRC program for their support. All authors have contributed equally to the conception, development, analysis of the project and the results, and to the development of the manuscript. On behalf of all coauthors, I declare that the results presented in this manuscript are original and the material has not been/will not be submitted to another journal.

Appendices

A1: details of the finite element mesh

Quadratic discretization has been used in the analysis. In terms of meshing, the maximum element size has been restricted to $h/20$. As it is seen in the results section, we use a truncated pyramid architecture for the composite with piezoelectric inclusions of random shape within a matrix (for a quick reference, see Fig. 3(a)). In the case of the composite architecture with maximum inclusion concentration, we have in total 28473 degrees of freedom. In the case of the minimum inclusion concentration (one inclusion), we have a total of 15009 degrees of freedom. The corresponding number of elements in the mesh are 3204 and 2252, respectively, for the composite architecture with maximum and minimum inclusion concentrations as considered here. We additionally point out that it is known that handling higher order derivatives in finite element implementations is connected with a number of reported challenges (e.g., strain gradients, in the case of flexoelectricity) [22]. In the process of optimizing the mess in our case, this is translated to a particular limit beyond which the mesh refinement could not be carried out. It is anticipated due to the ill-posed nature of numerical differentiation well elucidated in the literature (e.g., [A1]). As a practical criterion here, we stopped the mesh refinement at a level where reasonable agreement with the published numerical data was achieved [11].

[A1] Wang, Z., Wang, H., and Qiu, S., A new method for numerical differentiation based on direct and inverse problems of partial differential equations, Applied Mathematics Letters, 43, 61-67, 2015.

A2: the effective elastic and dielectric coefficients of CNT-modified epoxy matrices

The effective Young's modulus and Poisson's ratio of the epoxy matrix, with pristine moduli $E_m = 3.5$ GPa and $\nu_m = 0.35$, modified by uniform addition of (15,15) multiwalled carbon nanotubes (MWCNTs) with a volume fraction f_{CNT}, is shown in Fig. AF1(a)–(c). The matrix is elastically anisotropic due to the random orientation of the nanotubes. Therefore, the elastic properties are computed using the Lame's parameters λ_m and μ_m as highlighted in Section 2.2. The effective elastic coefficients are obtained by micromechanics approaches described in [37]. The effective permittivity of the composite matrix is computed based on the percolative relation $\varepsilon_M^{eff} = \varepsilon_M(\frac{f_p}{f_p - f_{CNT}})^p$, where ε_M is the relative permittivity of the pristine matrix, f_p is the percolation threshold for the nanotubes in the matrix, and p is the critical exponent characterizing the percolation behavior. We have assumed $f_p = 0.7\%$ and $p = 1.0$.

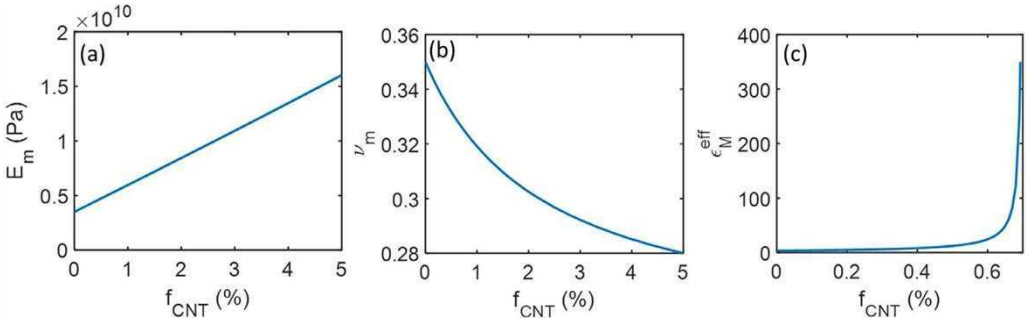

Fig. AF1. The effective (a) Young's modulus, (b) Poisson's ratio, and (c) relative permittivity of the epoxy matrix modified by addition of (15,15) MWCNTs, as a function of the nanotube volume fraction f_{CNT}.

References

[1] Ibn-Mohammed T, Koh S, Reaney I, Sinclair D, Mustapha K, Acquaye A, Wang D. Are lead-free piezoelectrics more environmentally friendly? MRS Commun 2017;7:1–7.
[2] Maurya D, Peddigari M, Kang M-G, Geng LD, Sharpes N, Annapureddy V, Palneedi H, Sriramdas R, Yan Y, Song H-C. Lead-free piezoelectric materials and composites for high power density energy harvesting. J Mater Res 2018;33:2235–63.
[3] Kim H, Torres F, Islam MT, Islam MD, Chavez LA, Garcia Rosales CA, Wilburn BR, Stewart CM, Noveron JC, Tseng T-LB, Lin Y. Increased piezoelectric response in functional nanocomposites through multiwall carbon nanotube interface and fused-deposition modeling three-dimensional printing. MRS Commun 2017;7:960–6.
[4] Zheng P, Zhang J, Tan Y, Wang C. Grain-size effects on dielectric and piezoelectric properties of poled BaTiO3 ceramics. Acta Mater 2012;60:5022–30.
[5] Yudin P, Tagantsev A. Fundamentals of flexoelectricity in solids. Nanotechnology 2013;24:432001.
[6] Zubko P, Catalan G, Tagantsev AK. Flexoelectric effect in solids. Annu Rev Mater Res 2013;43(1):387–421.
[7] Wang X. Piezoelectric nanogenerators—harvesting ambient mechanical energy at the nanometer scale. Nano Energy 2012;1:13–24.
[8] Hu T, Deng Q, Liang X, Shen S. Measuring the flexoelectric coefficient of bulk barium titanate from a shock wave experiment. J Appl Phys 2017;122:055106.
[9] Ma W, Cross LE. Flexoelectricity of barium titanate. Appl Phys Lett 2006;88:232902.
[10] Abdollahi A, Millán D, Peco C, Arroyo M, Arias I. Revisiting pyramid compression to quantify flexoelectricity: a three-dimensional simulation study. Phys Rev B 2015;91:104103.
[11] Abdollahi A, Peco C, Millan D, Arroyo M, Arias I. Computational evaluation of the flexoelectric effect in dielectric solids. J Appl Phys 2014;116:093502.
[12] Ghasemi H, Park HS, Rabczuk T. A level-set based IGA formulation for topology optimization of flexoelectric materials. Comput Meth Appl Mech Eng 2017;313:239–58.
[13] Zhu W, Fu JY, Li N, Cross L. Piezoelectric composite based on the enhanced flexoelectric effects. Appl Phys Lett 2006;89:192904.
[14] Huang W, Shu L, Ryung KS, Zhang S, Yuan F-G, Jiang X. Fabrication and measurement of a flexoelectric micro-pyramid composite. AIP Adv 2014;4:127115.
[15] Jiang X, Huang W, Zhang S. Flexoelectric nano-generator: materials, structures and devices. Nano Energy 2013;2:1079–92.
[16] Ghasemi H, Park HS, Rabczuk T. A multi-material level set-based topology optimization of flexoelectric composites. Comput Meth Appl Mech Eng 2018;332:47–62.
[17] Kundalwal S, Shingare K, Rathi A. Effect of flexoelectricity on the electromechanical response of graphene nanocomposite beam. Int J Mech Mater Des 2019;15:447–70.
[18] Shingare K, Kundalwal S. Static and dynamic response of graphene nanocomposite plates with flexoelectric effect. Mech Mater 2019;134:69–84.
[19] Thanh C-L, Ferreira AJM, Abdel WM. A refined size-dependent couple stress theory for laminated composite micro-plates using isogeometric analysis. Thin-Walled Struct 2019;145:106427.
[20] Thanh C-L, Tran LV, Vu-Huu T, Abdel-Wahab M. The size-dependent thermal bending and buckling analyses of composite laminate microplate based on new modified couple stress theory and isogeometric analysis. Comput Meth Appl Mech Eng 2019;350:337–61.
[21] Thanh C-L, Tran LV, Vu-Huu T, Nguyen-Xuan H, Abdel-Wahab M. Size-dependent nonlinear analysis and damping responses of FG-CNTRC micro-plates. Comput Meth Appl Mech Eng 2019;353:253–76.
[22] He B, Javvaji B, Zhuang X. Characterizing flexoelectricity in composite material using the element-free galerkin method. Energies 2019;12:271.
[23] Sharma N, Landis CM, Sharma P. Piezoelectric thin-film superlattices without using piezoelectric materials. J Appl Phys 2010;108:024304.
[24] Liu C, Wang J. Size-dependent electromechanical properties in piezoelectric superlattices due to flexoelectric effect. Theor Appl Mech Lett 2017;7:88–92.
[25] Abdollahi A, Arias I. Constructive and destructive interplay between piezoelectricity and flexoelectricity in flexural sensors and actuators. J Appl Mech 2015;82:121003.
[26] Bahrami-Samani M, Patil SR, Melnik R. Higher-order nonlinear electromechanical effects in wurtzite GaN/AlN quantum dots. J Phys 2010;22:495301.
[27] Joshi SP. Non-linear constitutive relations for piezoceramic materials. Smart Mater Struct 1992;1:80.
[28] Kuang Z-b. Internal energy variational principles and governing equations in electroelastic analysis. Int J Solids Struct 2009;46:902–11.
[29] Avila H, Ramajo L, Goes M, Reboredo M, Castro M, Parra R. Dielectric behavior of epoxy/BaTiO3 composites using nanostructured ceramic fibers obtained by electrospinning. ACS Appl Mater Interfaces 2013;5:505–10.
[30] James NK, Van Den Ende D, Lafont U, van der Zwaag S, Groen WA. Piezoelectric and mechanical properties of structured PZT–epoxy composites. J Mater Res 2013;28:635–41.
[31] Nguyen TD, Mao S, Yeh YW, Purohit PK, McAlpine MC. Nanoscale flexoelectricity. Adv Mater 2013;25:946–74.
[32] Li JY. The effective electroelastic moduli of textured piezoelectric polycrystalline aggregates. J Mech Phys Solids 2000;48:529–52.
[33] Johnston I, McCluskey D, Tan C, Tracey M. Mechanical characterization of bulk Sylgard 184 for microfluidics and microengineering. J Micromech Microeng 2014;24:035017.
[34] Chu B, Salem D. Flexoelectricity in several thermoplastic and thermosetting polymers. Appl Phys Lett 2012;101:103905.
[35] Wang J, Meng F, Ma X, Xu M, Chen L. Lattice, elastic, polarization, and electrostrictive properties of BaTiO 3 from first-principles. J Appl Phys 2010;108:034107.
[36] Zhenyi M, Scheinbeim JI, Lee JW, Newman BA. High field electrostrictive response of polymers. J Polym Sci Part B 1994;32:2721–31.
[37] Rodríguez-Tembleque L, García-Macías E, Sáez A. CNT-polymer nanocomposites under frictional contact conditions. Compos Part B 2018;154:114–27.
[38] Li J, Ma PC, Chow WS, To CK, Tang BZ, Kim JK. Correlations between percolation threshold, dispersion state, and aspect ratio of carbon nanotubes. Adv Funct Mater 2007;17:3207–15.
[39] Wang F, Wang J-W, Li S-Q, Xiao J. Dielectric properties of epoxy composites with modified multiwalled carbon nanotubes. Polym Bull 2009;63:101–10.
[40] Bao H-D, Sun Y, Xiong Z-Y, Guo Z-X, Yu J. Effects of the dispersion state and aspect ratio of carbon nanotubes on their electrical percolation threshold in a polymer. J Appl Polym Sci 2013;128:735–40.
[41] Li Q, Xue Q, Hao L, Gao X, Zheng Q. Large dielectric constant of the chemically functionalized carbon nanotube/polymer composites. Compos Sci Technol 2008;68:2290–6.
[42] Kvashnin AG, Sorokin PB, Yakobson BI. Flexoelectricity in carbon nanostructures: nanotubes, fullerenes, and nanocones. J Phys Chem Lett 2015;6:2740–4.
[43] Hwang GT, Byun M, Jeong CK, Lee KJ. Flexible piezoelectric thin-film energy harvesters and nanosensors for biomedical applications. Adv Healthc Mater 2015;4:646–58.
[44] Lee M, Chen CY, Wang S, Cha SN, Park YJ, Kim JM, Chou LJ, Wang ZL. A hybrid piezoelectric structure for wearable nanogenerators. Adv Mater 2012;24:1759–64.